Structural Insights into the Mechanism of the PLP Synthase Holoenzyme from *Thermotoga maritima*[†,‡]

Fairuz Zein, Yan Zhang, You-Na Kang, Kristin Burns, Tadhg P. Begley,* and Steven E. Ealick*

Department of Chemistry and Chemical Biology, Cornell University, Ithaca, New York 14853

Received July 19, 2006; Revised Manuscript Received September 5, 2006

ABSTRACT: Pyridoxal 5′-phosphate (PLP) is the biologically active form of vitamin B_6 and is an important cofactor for several of the enzymes involved in the metabolism of amine-containing natural products such as amino acids and amino sugars. The PLP synthase holoenzyme consists of two subunits: YaaD catalyzes the condensation of ribulose 5-phosphate, glyceraldehyde-3-phosphate, and ammonia, and YaaE catalyzes the production of ammonia from glutamine. Here we describe the structure of the PLP synthase complex (YaaD−YaaE) from *Thermotoga maritima* at 2.9 Å resolution. This complex consists of a core of 12 YaaD monomers with 12 noninteracting YaaE monomers attached to the core. Compared with the previously published structure of PdxS (a YaaD ortholog in *Geobacillus stearothermophilus*), the N-terminus (1−18), which includes helix α0, the β2−α2 loop (46−56), which includes new helix α2a, and the C-terminus (270−280) of YaaD are ordered in the complex but disordered in PdxS. A ribulose 5-phosphate is bound to YaaD via an imine with Lys82. Previous studies have demonstrated a similar imine at Lys149 and not at Lys81 (equivalent to Lys150 and Lys82 in *T. maritima*) for the *Bacillus subtilis* enzyme suggesting the possibility that two separate sites on YaaD are involved in PLP formation. A phosphate from the crystallization solution is found bound to YaaD and also serves as a marker for a possible second active site. An ammonia channel that connects the active site of YaaE with the ribulose 5-phosphate binding site was identified. This channel is similar to one found in imidazole glycerol phosphate synthase; however, when the β-barrels of the two complexes are superimposed, the glutaminase domains are rotated by about 180° with respect to each other.

Pyridoxal 5′-phosphate (**4**, PLP)[1] is the biologically active form of vitamin B_6 and is an important cofactor for several of the enzymes involved in the metabolism of amine-containing natural products such as amino acids and amino sugars (*1*−*4*). There are two distinct PLP biosynthetic pathways that have not yet been found to coexist in the same organism (*5*). The *Escherichia coli* pathway has been extensively studied (*6*−*12*). In this pathway, PdxJ catalyzes the formation of pyridoxine 5′-phosphate (**3**, PNP) from 3-phosphohydroxy-1-aminoacetone **2** and 1-deoxy-D-xyulose 5-phosphate **1**. This is then oxidized to PLP **4** by PdxH (Scheme 1). In the alternative pathway, PLP is formed from ribose 5-phosphate (**5**, R5P), glyceraldehyde 3-phosphate (**6**, G3P), and ammonia formed by the hydrolysis of glutamine (*13*−*18*) (Scheme 1). The required genes in *Bacillus subtilis* are YaaD and YaaE. Orthologs of YaaD (Snz, PdxS, and Pdx1) and YaaE (Sno, PdxT, and Pdx2) are widely distributed in bacteria, eukarya, and archaea (*19*−*21*). YaaD shows an unusually high degree of sequence conservation with approximately 28% of its residues (78/280) absolutely conserved over 73 amino acid sequences. The structure of PdxS from *Geobacillus stearothermophilus* has been previously reported (*22*). This protein is a dodecamer with 622 point symmetry. The monomers have a classic $(\beta/\alpha)_8$ fold with the axis of each β-barrel approximately perpendicular to the molecular sixfold axis. YaaE is a class I amidotransferase (*23*, *24*) characterized by a conserved Glu-His-Cys (*25*). The structures of YaaE from *B. subtilis* (*17*) and *Bacillus stearothermophilus* (PDB ID 1Q7R) have been reported as well as the YaaE ortholog, Pdx2, from *Plasmodium falciparum* (*26*). YaaE has an (αβα) three-layer sandwich fold and a highly conserved glutamine binding site. YaaD and YaaE form a complex (*16*) in which the ammonia generated by hydrolysis of glutamine is channeled to the YaaD active site.

Here we report the three-dimensional structure of the *Thermotoga maritima* PLP synthase complex (YaaD/YaaE) solved to a resolution of 2.9 Å. The structure suggests a possible channel through which ammonia could travel from its site of generation on YaaE to the PLP forming site on YaaD. Comparison of the YaaD subunit with the structure of the previously solved, unliganded PdxS from *G. stearothermophilus* (PDB ID 1ZNN) and the structure of the YaaE subunit with the structures of YaaE from *B. subtilis* (PDB ID 1R9G) and HisHF from *T. maritima* (PDB ID 1JVN) provides information about structural and functional changes

[†] This work was supported by National Institutes of Health Grants DK44083 (T.P.B.) and DK67081 and RR015301 (S.E.E.).

[‡] The Brookhaven Protein Data Bank code for PLP synthase is 2ISS.

* Corresponding authors. Telephone: (607) 255-7961. Fax: (607) 255-1227. E-mail: see3@cornell.edu or tpb2@cornell.edu.

[1] Abbreviations: PLP, pyridoxal 5′-phosphate; PNP, pyridoxine 5′-phosphate; DXP, deoxy-D-xylulose-5-phosphate; RBP, ribulose-5-phosphate; R5P, ribose 5-phosphate; G3P, glyceraldehyde 3-phosphate; DHAP, dihydroxyacetone phosphate; acivicin, (α*S*,5*S*)-α-amino-3-chloro-4,5-dihydro-5-isoxazoleacetic acid; MPD, 2-methyl-2,4-pentanediol; APS, Advanced Photon Source; rmsd, root mean square deviation.

10.1021/bi061464y CCC: $33.50
Published on Web 11/14/2006

Scheme 1

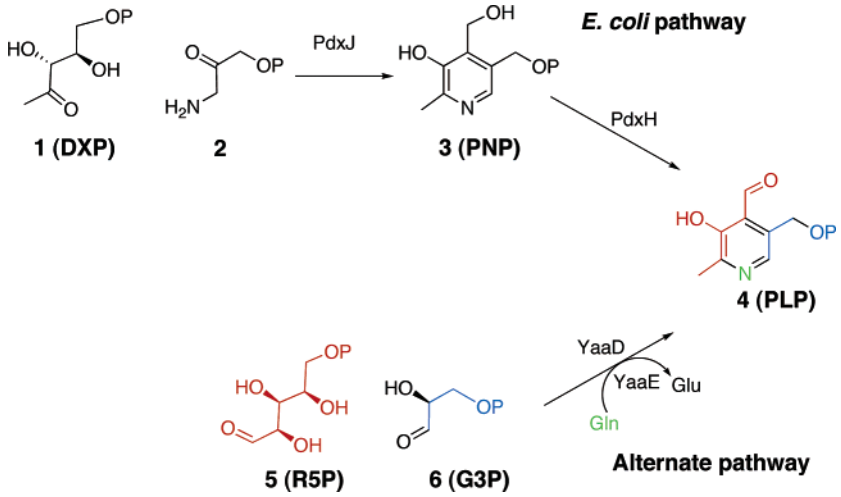

that occur with the binding of ribulose 5-phosphate (RBP), an early intermediate in the PLP synthase reaction. The identification of a new ribulose phosphate binding site on YaaD suggests that PLP synthase may use two separate active sites to catalyze the complex chemistry involved in the formation of PLP.

METHODS AND MATERIALS

Molecular Cloning. Standard methods were used for DNA restriction endonuclease digestion, ligation, and transformation of DNA. Genomic DNA and plasmid DNA were purified with a Wizard Plus SV genomic DNA kit and a DNA Miniprep kit (Promega), respectively. DNA fragments were separated by agarose gel electrophoresis, excised, and purified with the QiaExII (Qiagen). *E. coli* strain DH5α was used as a recipient for transformation during plasmid construction and for plasmid propagation and storage. *E. coli* Tuner (DE3) (Novagen) was used as a host strain for the overexpression of proteins. A Perkin-Elmer GeneAmp PCR System 2400 apparatus and Platinum Pfx DNA polymerase (Invitrogen) were used for PCR. *T. maritima* DSM3109 genomic DNA was used as a template for PCR. Primer synthesis and DNA sequencing were performed by the Bioresource Center at Cornell University. Primers introduced *Nde*I and *Xho*I restriction enzyme sites at the 5′ and 3′ ends, respectively. For YaaE, 5′-AGA GGG TGG TAA CAT ATG AAG ATA GGC GTT CTG GGT G-3′ (*Nde*I site is underlined) and 5′-ACC TGC CTC GAG AAC GAT ACT GGC TAT TCG TTC ACG-3′ (*Xho*I site is underlined) were used as the primer pair. For YaaD, 5′-AGT GAG GAG GTG AAC CAT ATG GAA ATC AAA AAG GGT ACC-3′ (*Nde*I site is underlined) and 5′-CAC CAT GTC CAG CTG CTC GAG AAG TTT CAC TAT CAG-3′ (*Xho*I site is underlined) were used as the primer pair. The PCR product was digested with *Nde*I and *Xho*I and ligated into similarly digested pET-28a (Novagen) to give pCLK1540 and pCLK1541, respectively.

Expression and Purification. For the overexpression and purification of *T. maritima* YaaD and YaaE, their corresponding overexpression plasmids (pCLK1540 and pCLK1541) were transformed into competent *E. coli* Tuner (DE3) cells, and the transformed cells were grown at 37 °C in M9 minimal medium supplemented with glucose, $MgSO_4$, and $CaCl_2$, containing 50 mg/L of kanamycin. To induce the overexpression of proteins, isopropyl-β-D-thiogalactopyranoside was added to the culture when the optical density at 595 nm reached 0.5 to achieve a final concentration of 1 mM. Culture growth was continued for 6 h at 25 °C, after which the cells were harvested and stored at −20 °C until further use. The cell pellets from both YaaD and YaaE were resuspended together, and the proteins copurified according to a Qiagen protocol for the purification of His-tagged proteins. The eluted protein complex was desalted into 20 mM Tris-HCl, pH 8, using a PD-10 column (Amersham Pharmacia), concentrated, and stored at 4 °C.

Crystallization of the PLP Synthase Complex. The PLP synthase complex was crystallized at 22 °C using the hanging drop vapor diffusion method. Each drop contained 2 μL of protein solution and 2 μL of reservoir solution. The protein solution in 20 mM Tris-HCl, pH 8.0, contained 7 mg/mL PLP synthase, 4 mM RBP, 4 mM dihydroxyacetone phosphate (DHAP), and 4 mM (α*S*,5*S*)-α-amino-3-chloro-4,5-dihydro-5-isoxazoleacetic acid (acivicin, an inhibitor of the glutaminase activity). The reservoir solution for the optimized conditions contained 0.8 M disodium hydrogen phosphate, 1.2 M potassium dihydrogen phosphate, and 0.2 M lithium sulfate at pH 6.1. Crystals appeared in 3 days and grew over 7 days to their maximum size (0.1 mm × 0.1 mm × 0.1 mm). The crystals belong to the orthorhombic space group *I*222 with unit cell dimensions $a = 92.5$ Å, $b = 204.1$ Å, and $c = 221.3$ Å . This corresponds to a solvent content of 59% with three YaaD monomers and three YaaE monomers per asymmetric unit.

X-ray Data Collection and Processing. The data were collected on a flash frozen crystal at cryogenic temperatures. The crystals were cryoprotected by a quick dip in a paratone and paraffin mixture with a v/v ratio of 1:2 and then flash frozen in liquid nitrogen. Monochromatic X-ray intensity data were measured at the Advanced Photon Source on the NE-CAT 24-ID-C beam line using a Quantum-315 CCD detector (Area Detector Systems Corp.). Data were collected at a wavelength of 0.979 Å over a range of 130° using 2 s exposures for each 0.5° oscillation at a crystal-to-detector distance of 350 mm. The HKL2000 suite (*27*) of programs was used for integration and scaling of data. Details of the data collection and processing are given in Table 1.

Table 1: Summary of Crystallographic Data and X-ray Intensity Data Collection

X-ray source	APS (24-ID-C)
space group	*I*222
unit cell parameters (Å)	$a = 92.5$, $b = 204.1$, $c = 221.3$
asymmetric unit	3 YaaD, 3 YaaE
resolution limit (Å)	50−2.9 (3.0−2.9)[a]
measured reflns	181201 (18229)[a]
unique reflns	45755 (4579)[a]
avg I/σ	14.33 (3.14)[a]
redundancy	4.0 (4.0)
completeness (%)	97.1 (98.6)
R_{sym}[b] (%)	8.7 (45.6)

[a] The numbers in parentheses are for the highest resolution shell. [b] $R_{sym} = \sum\sum_i|I_i - \langle I\rangle|/\sum\langle I\rangle$, where $\langle I\rangle$ is the mean intensity of the N reflections with intensities I_i and common indices *hkl*.

Structure Determination and Model Refinement. The structure of the PLP synthase complex (YaaD/YaaE) was determined by molecular replacement with the Crystallography & NMR System (CNS) software package (*28*) using the structure of PLP synthase PdxS from *G. stearothermophilus* (PDB ID 1ZNN) as a search model. A solution with a correlation coefficient of 0.3 was obtained using the data between 10 and 4 Å resolution. An initial electron density map clearly showed the presence of YaaE bound to each YaaD subunit. The molecular model of YaaE was built assisted by the structure of YaaE from *B. subtilis* (PDB ID 1R9G). The final model contains three YaaD/YaaE complexes per asymmetric unit. The structure of YaaD/YaaE was refined by consecutive cycles of simulated annealing, energy minimization, and temperature factor refinements using CNS (*28*) and manual rebuilding by the programs O (*29*) and COOT (*30*). A total of 5% of the reflections were excluded for the calculation of R_{free}. Tight noncrystallographic symmetry (NCS) restraints were applied throughout the refinements. NCS map averaging with RAVE (*31*) and solvent flattening with CNS (*28*) improved the electron density maps. Water molecules were picked automatically using CNS (*28*) and were manually inspected by O (*29*) and COOT (*30*). The final model was assessed with PROCHECK (*32*) and MolProbity (*33*). The refinement statistics of the final model are summarized in Table 2.

Mutagenesis of B. subtilis YaaD. Lys81 was mutated to alanine from YaaD.28 (*15*) using the following primers: 5′-(for)-ATC CCG GTA ATG GCA GCA GCG CGT ATC GGA CAT-3′; 5′(rev)-ATG TCC GAT ACG CGC TGC TGC CAT TAC CGG GAT-3′. Lys149 was mutated to alanine using the following primers: 5′(for)-GGT GCT TCT ATG CTT CGC ACA GCA GGT GAG CCT GGA ACA GG-3′; 5′(rev)-CC TGT TCC AGG CTC ACC TGC TGT GCG AAG CAT AGA AGC ACC-3′. A Stratagene site-directed mutagenesis kit was used to amplify the plasmid DNA. Expression and purification proceeded as for wild-type YaaD.

PLP Synthase Activity. Mutant YaaD (300 μg), YaaE (300 μg), 4 mM R5P, 4 mM DHAP, and 4 mM glutamine were incubated for 16 h at 37 °C in 350 μL of 50 mM phosphate, pH 8. Activity was monitored by UV−vis.

Pentose Isomerization. Mutant YaaD (500 μg) was incubated with 2.5 mM R5P in 50 mM phosphate, pH 8, in D_2O. The reaction was monitored by 600 MHz NMR.

Figure Preparation. MOLSCRIPT (*34*), RASTER3D (*35*), and PyMOL (*36*) were used to prepare the figures.

Table 2: Summary of Structure Refinement

resolution (Å)	500−2.9 (3.0−2.9)[a]
total no. of non-hydrogen atoms	
no. of protein atoms	10813
no. of water molecules	38
no. of reflns in refinement	43430 (4055)[a]
no. of reflns in test set	2178
R factor (%)[b]	21.34
R_{free} (%)[c]	23.60
rmsd from ideal geometry	
bonds (Å)	0.006
angles (deg)	1.29
Ramachandran plot[d]	
most favored region (%)	92.5/85.9
additional allowed region (%)	7.4/13.5
generously allowed region (%)	0.1/0
disallowed region (%)	0/0.6
average B factors (Å^2)[d]	46.9/59.4

[a] The numbers in parentheses are for the highest resolution shell. [b] R factor $= \sum_{hkl}||F_{obs}| - k|F_{calc}||/\sum_{hkl}|F_{obs}|$, where F_{obs} and F_{calc} are the observed and calculated structure factors, respectively. [c] R_{free} was calculated using 5% of all reflections that were excluded from refinement. [d] The first number is for YaaD monomers, and the second is for YaaE monomers.

RESULTS

Quality of the Structure. The crystal structure of the PLP synthase complex (YaaD−YaaE) was determined at a resolution of 2.9 Å. The asymmetric unit contains three monomers of YaaD (denoted as A, B, and C) and three monomers of YaaE (denoted as D, E, and F). The structure shows a high overall *B*-factor consistent with the resolution of the diffraction pattern; however, the main structural features including the R5P ligand bound at the active site of each YaaD monomer are clear. Each monomer of YaaD is complete except for residues 281−293 at the C terminus. The Ramachandran plot shows no residues in the disallowed region. Each monomer of YaaE is complete except for residues 89−92, which are located in a loop between β5 and β6. Compared with the YaaD monomers, the YaaE monomers show higher *B*-factors (59 Å^2 compared with 47 Å^2 for YaaD) and show more residues in the additionally allowed region of the Ramachandran plot (13.5% compared with 7.4% for YaaD). The catalytic Cys78 residue of YaaE is in the disallowed region for all three monomers. This is typical for triad glutaminases.

Structure of the YaaD/YaaE Protomer. The protomer of the PLP synthase complex is the YaaD/YaaE heterodimer (Figure 1a). The architecture of the YaaD monomer is based on the classic $(\beta/\alpha)_8$ barrel fold (Figure 1b) and is very similar to the PdxS monomer, which shares 71% sequence identity with YaaD, in the recently published structure of the PLP synthase core (*22*). Modifications to the $(\beta/\alpha)_8$ barrel are an eight-residue N-terminal helix (α0), which caps the bottom of the β-barrel, helix α2a in the β2 and α2 loop, helices α6a and α6b inserted between helix α6 and strand β7, a 3_{10}-helix preceding α8, and one additional α-helix (α8a) following helix α8. Helix α4 (119−121) is a 3_{10}-helix, but the designation α4 is retained for consistency. The main differences between the structure of YaaD in complex with YaaE and the structure of PdxS are that the N-terminal tail (1−7), helix α0 (8−16), residues 46−56, including helix α2a, in the connection between β2 and α2a, and part of the C-terminal tail (270−280) are ordered in YaaD, whereas

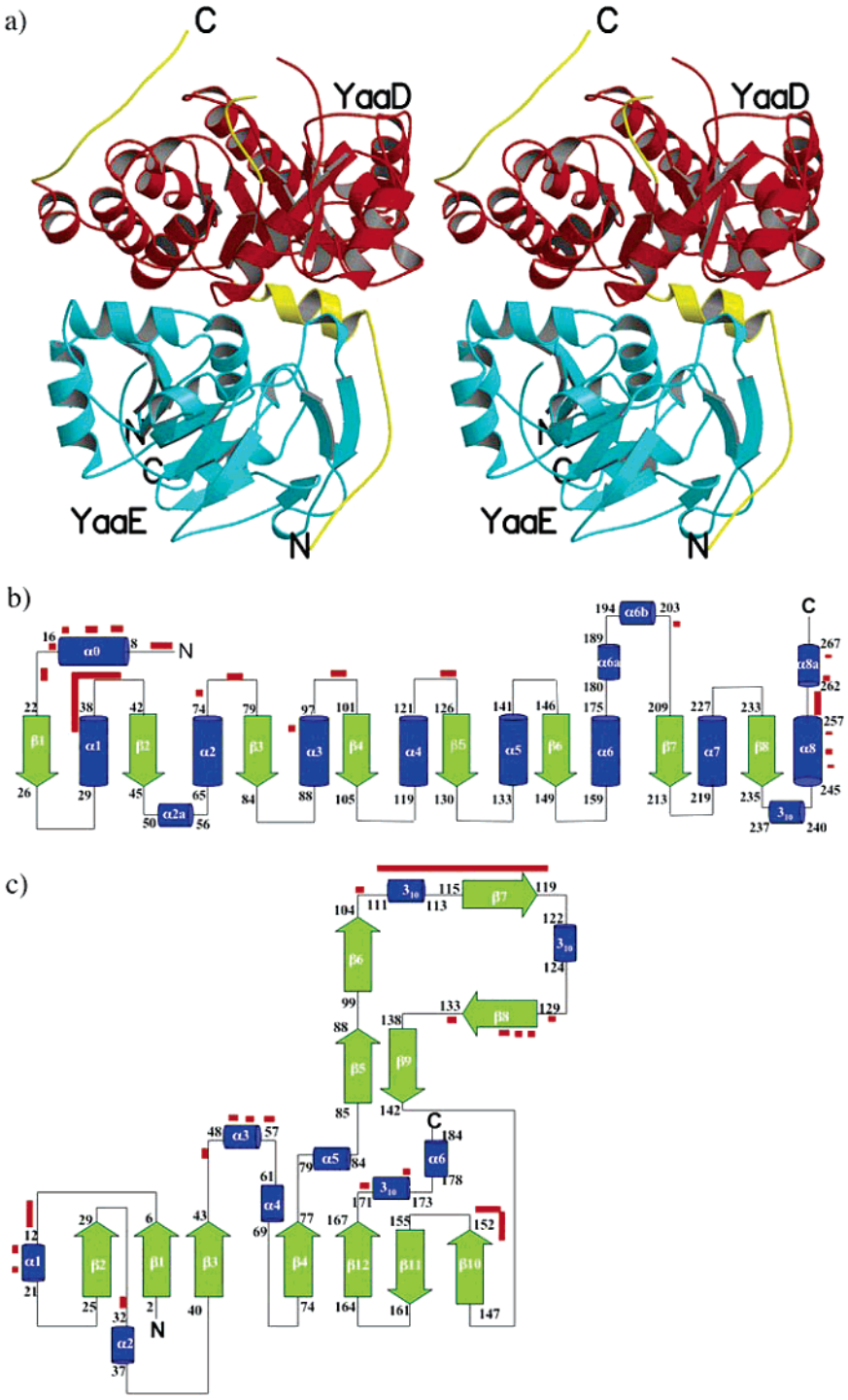

FIGURE 1: Structure of the YaaD/YaaE protomer. (a) Stereoview of the protomer. Red indicates regions of YaaD that are similar to PdxS. Yellow indicates regions of YaaD that are disordered in PdxS. Blue indicates YaaE. (b) Topology diagram for YaaD. (c) Topology diagram for YaaE. The secondary structural elements are labeled, and residue numbers for the beginning and end of each element are given. Red lines indicate regions that form the interface of the YaaD/YaaE heterodimer.

these regions were disordered in PdxS. The ordered regions are mostly involved in interactions with YaaE, although the C-terminal tail bridges adjacent YaaD monomers (see below).

YaaE is an α/β three-layer sandwich containing twelve β-strands, six α-helices, and three 3_{10}-helices (Figure 1c) and is characteristic of class I amidotransferases. The structure of YaaE in complex with YaaD is similar to the structures of YaaE from *B. subtilis* (*17*), YaaE from *B. stearothermophilus* (PDB ID 1Q7R), and Pdx2 from *P. falciparum* (*26*). The class I amidotransferases contain a characteristic Glu-His-Cys catalytic triad, which in *T. maritima* YaaE is Glu172-His170-Cys78. His170 and Glu172 are located at the beginning of a 3_{10}-helix following β12, and Cys78 is located at the end of strand β4. Of the many combinations of YaaD, YaaE, substrates, products, and inhibitors tried, crystals were obtained only in the presence of RBP, DHAP, and acivicin. Although acivicin, which is expected to covalently bind to Cys78, was present in the crystallization

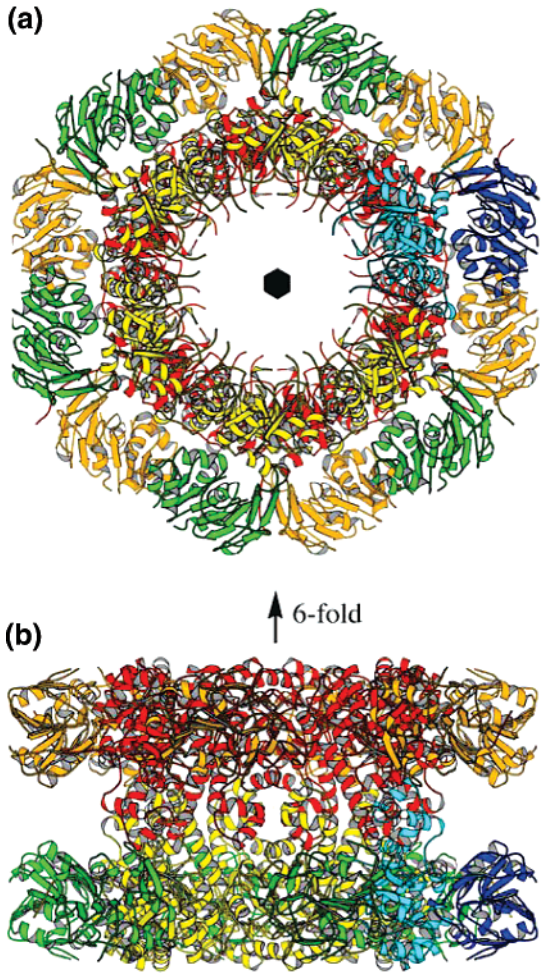

FIGURE 2: Structure of the PLP synthase dodecamer. (a) View down the molecular sixfold axis. (b) View perpendicular to the sixfold. One YaaD/YaaE protomer is highlighted with YaaD shown in light blue and YaaE shown in dark blue. For all other monomers, yellow and red indicate the YaaD subunits in the two hexameric layers that join face-to-face to form the dodecamer. Green and orange represent the YaaE monomers for the yellow and red hexamers, respectively. The dimensions of the complex are about 160 Å in the maximum dimension perpendicular to the sixfold axis and about 90 Å thick in the direction parallel to the sixfold axis. The central channel along the sixfold axis is approximately 40 Å in diameter.

solution, the inhibitor was not observed in the YaaE active site in the crystal structure.

Structure of the PLP Synthase (YaaD/YaaE) Complex. The PLP synthase complex consists of 12 monomers of YaaD/YaaE heterodimers (Figure 2). The core of the PLP synthase complex is formed by a dodecamer of YaaD monomers and is similar to the recently reported structure of the PdxS dodecamer from *G. stearothermophilus* (*22*). The YaaD dodecamer has approximate dimensions 160 Å in the maximum dimension perpendicular to the sixfold axis and about 90 Å thick in the direction parallel to the sixfold axis. The top (C-terminal end of the β-barrel) of each YaaD monomer is oriented to face the central channel. Approximately 6040 Å^2 of surface area for each YaaD monomer is buried in the formation of the PLP synthase dodecamer core. The interactions responsible for stabilizing the core are essentially the same as those reported for the PdxS dodecamer (*22*).

Twelve YaaE monomers decorate the surface of the YaaD dodecamer. While there are extensive interactions between YaaD and YaaE, there are no interactions between YaaE monomers. A total of 3740 Å^2 of surface area is buried in each YaaD/YaaE interface. Regions of YaaD involved in YaaD/YaaE interactions include the N-terminal tail, helix α0, loop α0$-\beta$1, the C-terminal end of α1, loop α1$-\beta$2, the C-terminal end of α2, loops α2$-\beta$3, α3$-\beta$4, α4$-\beta$5, and α6b$-\beta$7, α8, the α8$-\alpha$8a loop, and α8a (Figures 1b and 3). Regions of YaaE involved in the interface include the β1$-\alpha$1 loop, the N-terminus of α1, loops β2$-\alpha$2 and β3$-\alpha$3, α3, the β6-3_{10} loop, the 3_{10}-helix preceding β7, β7, the β7-3_{10} loop, the $3_{10}-\beta$8 loop, β8, loops β8$-\beta$9 and β10$-\beta$11, and the 3_{10}-helix following β12 (Figures 1c and 3). The interface involves 21 hydrogen bonds and salt bridges between Lys5 (YaaD) and Glu113 (YaaE), Lys19 (YaaD) and Glu14 (YaaE), Asp100 (YaaD) and Arg110 (YaaE), and Lys250 (YaaD) and Glu57 (YaaE).

RBP Binding Site. Figure 4a shows the RBP site of YaaD. Lys82 forms a Schiff base with the C2 carbonyl of RBP and stretches across the bottom (N-terminal end of the β-barrel). The amide nitrogen atoms of Gly215, Gly154, Gly236, and Ser237, and the side chain of Ser237 form hydrogen bonds with the phosphate oxygen atoms. Arg148 and Asp103 are hydrogen bonded with the C1 hydroxyl group, while Asp25 forms a hydrogen bond with the C3 hydroxyl group. Arg148 and Asp103 also form a salt bridge. The remaining residues in the RBP binding site are mostly hydrophobic and include Pro50, Val107, Leu46, Met44, and Leu108. All of the RBP binding site residues are strictly conserved. The RBP sites in adjacent YaaD monomers are about 30 Å apart.

Additional YaaD Phosphate Binding Site. A phosphate ion from the crystallization solutions is bound in each YaaD monomer (Figure 4b). The residues surrounding this phosphate site are His116 (loop β4$-\alpha$4), Arg131 (loop β5$-\alpha$5), Glu135, Arg138, and Arg139 (α5), Lys150 (β6$-\alpha$6), and Lys188 (α6a from a YaaD monomer located at the opposite hexamer). A similar phosphate binding site was observed in the structure of PdxS (*22*). Although the phosphate site is mostly exposed, it may represent the phosphate binding site of the second substrate (DHAP), the product, or an intermediate along the reaction coordinate.

Putative Ammonia Channel. The formation of PLP requires that the ammonia molecule generated in the YaaE active site be channeled without exposure to bulk solvent to the active site of YaaD. The most likely channel from YaaE to YaaD is shown in Figure 5a and is approximately 26 Å in length. The channel was constructed by identifying interior cavities that when connected together formed a continuous channel from the glutamine binding site of YaaE to the RBP binding site of YaaD. The interior side chains of the β-barrel and side chains near Cys78 (YaaE) are shown in Figure 5b. The channel originates at the YaaE active site where ammonia is generated by the hydrolysis of glutamine and travels across the YaaE and YaaD interface where it enters the bottom (N-terminal end) of the β-barrel of YaaD. Two absolutely conserved residues of YaaE, Glu47 and Arg135, may serve as a gate. Parts of the channel at the YaaD/YaaE interface are formed by α0 of YaaD, which is completely ordered in the complex structure but disordered in the structure of PdxS (*22*). The residues of the β-barrel core are

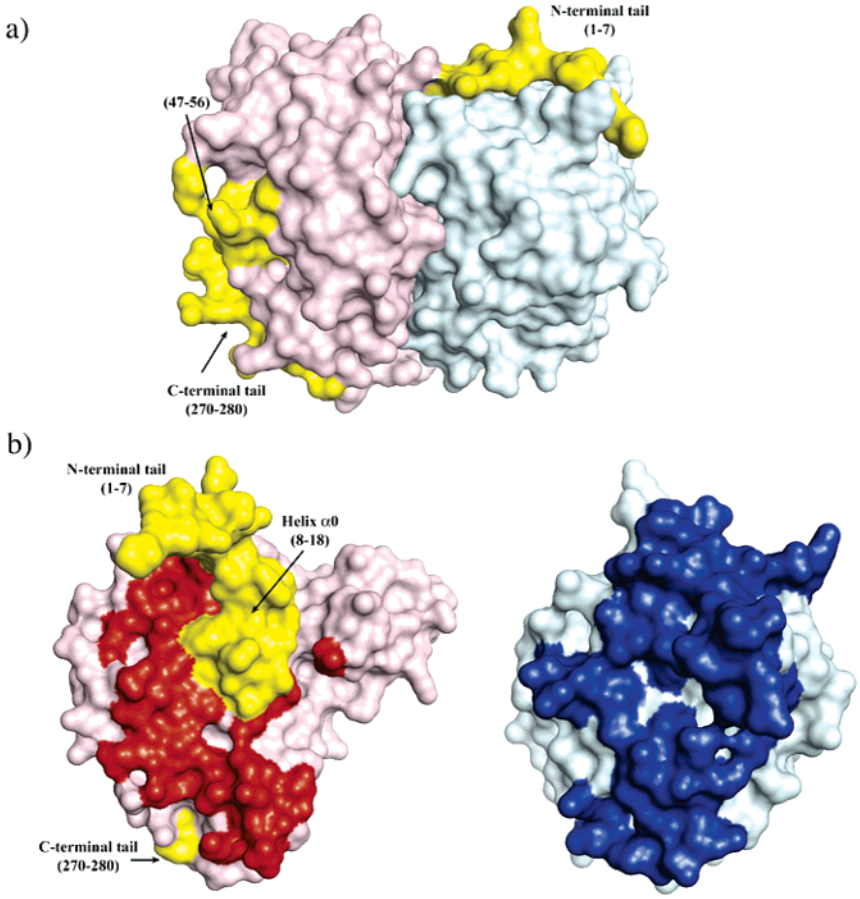

FIGURE 3: Surface representation of the YaaD/YaaE protomer. (a) YaaD/YaaE heterodimer. YaaD is colored in pink, YaaE is colored in light blue, and regions of YaaD corresponding to disordered regions of PdxS are colored in yellow and labeled. (b) Open book representation of YaaD (left) and YaaE (right). The color coding is the same as panel a, except the interface region of YaaD is shown in red and the interface region of YaaE is shown in blue. The yellow regions are also involved in monomer−monomer interactions.

mostly hydrophobic until the RBP binding site is reached. At that point RBP, Asp25, Asp103, and Arg148 block the channel.

Mutagenesis Studies. Lys149 of *B. subtilis* YaaD (equivalent to Lys150 in *T. maritima*) was previously identified by electrospray ionization Fourier transform mass spectrometry (ESI-FTMS) to be involved in adduct formation with RBP (*15*). In contrast, the structure described here shows that the invariant residue Lys82 of the *T. maritima* enzyme (equivalent to Lys81 in *B. subtilis*) is covalently bound to RBP at the C2 position. To determine the catalytic function of these two residues, the K81A and the K149A mutants of the *B. subtilis* enzyme were constructed (Table 3). Neither mutant catalyzed the formation of PLP. In addition, K81A does not catalyze the isomerization of R5P, while K149A catalyzes the isomerization of R5P three times faster than the wild-type enzyme.

DISCUSSION

Comparison with Other Structures. A DALI (*37*) comparison of the YaaD monomer with other structures resulted in a large number of hits. The most closely related eight structures are listed in Table 4. While these enzymes catalyze a diverse set of chemical reactions, it is interesting to note that YaaD/PdxS, ThiG, PdxJ, and HisH all catalyze the formation of heterocyclic rings using imine forming, tautomerization, and dehydration reactions. Not surprisingly, the YaaD ortholog PdxS from *G. stearothermophilus* (PDB ID 1ZNN) (*22*) is most similar to YaaD. In addition to being structurally similar, all the predicted active site residues of YaaD are also conserved in PdxS. Interestingly, the structure of PdxS contains a molecule of 2-methyl-2,4-pentanediol (MPD) and a nearby phosphate ion that superimpose closely with the RBP in YaaD (Figure 6). In YaaD, the RBP phosphate forms hydrogen bonds with the amide nitrogen atoms of Gly154, Gly215, Gly236, and Ser237 and the side chain of Ser237, while the sulfate in PdxS forms hydrogen bonds with the glycine amide nitrogen atoms of the absolutely conserved Gly153-Thr154-Gly155 loop, which correspond to Gly154-Thr155-Gly156 in YaaD. After structural alignment of the protein atoms, the sulfate is displaced from the RBP phosphate group by 2.6 Å. These observations suggest two different phosphate binding sites that could accommodate different intermediates or products along the reaction coordinate.

The second most similar structure to YaaD is triosephosphate isomerase (TIM, PDB ID 1HG3) (*38*), which catalyzes the interconversion of DHAP and G3P during glycolysis. Following TIM is thiamin phosphate synthase (TPS) (PDB ID 2TPS), which has thiamin phosphate bound in its active site (*39*). TPS catalyzes the coupling of 2-methyl-4-amino-5-hydroxymethylpyrimidine pyrophosphate with 4-methyl-5-(β-hydroxyethyl)thiazole phosphate to obtain thiamine phosphate. The next most closely related structure is ThiG (PDB ID ITYG) (*40*). ThiG is a thiazole synthase that catalyzes the formation of the thiamin thiazole from deoxy-

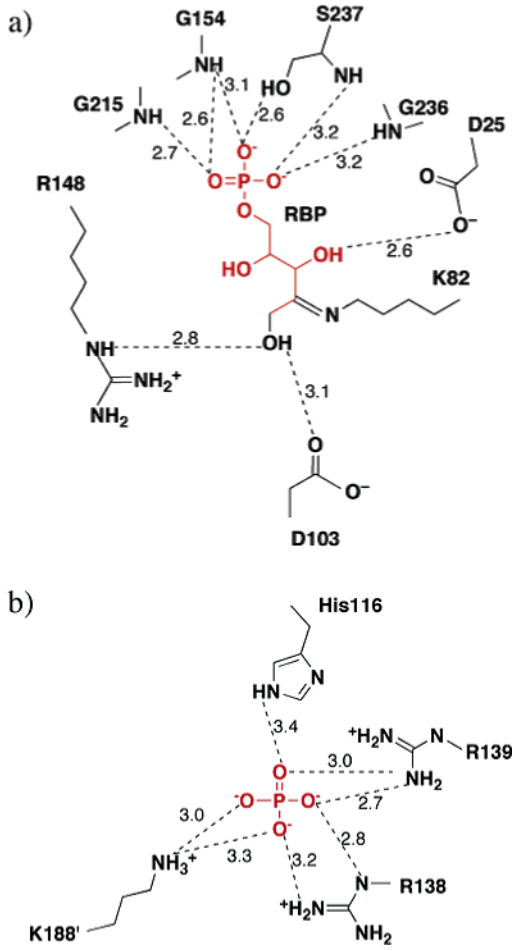

FIGURE 4: Ligand binding sites in YaaD. (a) Schematic diagram of the RBP binding site showing key hydrogen bonds. (b) Schematic diagram showing key hydrogen bonds of the phosphate binding site. Lys188′ comes from the adjacent YaaD monomer. The length of each hydrogen bond, shown with dotted lines, is given in Å.

D-xylulose 5-phosphate (DXP). Following ThiG is PNP synthase (PdxJ) (PDB ID 1HO1) (*41*). The YaaD (PdxS), TIM, TPS, ThiG, and PdxJ enzymes all have a phosphate ion corresponding to the phosphate of RBP bound in similar locations in the structures (Figure 7). This suggests that the phosphate binding site was conserved even while the active site was evolving to generate a diverse set of enzymatic activities.

PNP synthase catalyzes the condensation reaction between 1-deoxy-D-xylulose 5-phosphate and 1-aminoacetone 3-phosphate to form PNP. This structural similarity is remarkable because closely related mechanisms can be formulated for the YaaD and the PdxJ catalyzed reactions. However, this mechanistic similarity is not evident when the active sites of the two proteins are compared. When the structure of PNP synthase with bound PNP is superimposed on YaaD, atoms corresponding to C4, C5, and phosphate of RBP align with the triose derived (*13*) atoms C5, C5′, and phosphate of PNP, and there is no overlap between the RBP atoms and the DXP derived atoms. This suggests that the PNP forming site on PdxJ is distinct from the PLP forming site on YaaD.

A DALI search to obtain similar structures to that of YaaE produced a large number of hits. All of the top hits are class I amidotransferases with a conserved Glu-His-Cys catalytic triad.

Conformational Changes upon Complex Formation. Compared with the structure of PdxS, YaaD shows several changes upon complex formation (Figures 1 and 3). PdxS, which lacks bound substrates, products, or glutaminase (PdxT), differs from YaaD by being disordered at three regions: the N-terminus (1−18), the β2−α2 active site loop (46−56), and the C-terminus (270−280). These regions are all clearly visible in the YaaD/YaaE complex, which also includes a new secondary structural element, α0 (8−16). Helix α0 is involved in extensive interactions with YaaE and helps form one side of the proposed ammonia channel. Comparing YaaD with PdxS, a series of smaller conformational changes in the 3_{10}-helix (237−240), the β6−α6 loop, α8, and α8a connect adjacent active sites within the PLP synthase complex. In the structure of YaaD, residues 46−56 form an active site loop. Residues in PdxS equivalent to 50−56 are disordered and form helix α2a in YaaD. Gly57 and Gly58, which are seen in a different conformation in PdxS, follow this helix. The coil to helix transition and the GG switch provide a structural link between monomers related by the sixfold axis. Residues 48−52 of the active site loop in one monomer are in close contact with the 3_{10}-helix and the β6−α6 loop. The ordered C-terminus (270−280) is in close contact with the β6−α6 loop, α8a, and residues 57−59 of the active site loop of the adjacent monomer.

Comparison of the YaaD/YaaE Complex to the HisF/HisH Complex. YaaD is structurally homologous to HisF and YaaE is structurally homologous to HisH (*42*, *43*). Together HisF and HisH make up the components of imidazole glycerol phosphate synthase. In some organisms HisF and HisH are fused to form a bienzyme complex, whereas in other organisms HisF and HisH are separate genes and the protein complex forms after protein synthesis. In either case, the HisH/HisF interface is very similar (*42*, *43*). In an earlier paper, we attempted to model the YaaD/YaaE complex using HisF/HisH as a template (*17*). While the contact surfaces were correctly predicted, the relative orientation of YaaE relative to YaaD was not. A model of the PdxS/PdxT complex was also proposed (*22*).

Figure 8 shows a superposition of the imidazole glycerol phosphate synthase bienzyme (HisHF) and one protomer of YaaD/YaaE using only the atoms of YaaD and YaaE for the overlay. While in both structures the active site of the glutaminase domain is docked to the bottom (N-terminal end) of the β-barrel, the orientations of the two glutaminases are entirely different. Compared with YaaE, HisH is rotated about the β-barrel axis by about 180°. Another important difference is the presence of a four-residue gate at the N-terminal end of the β-barrel in HisF. YaaD lacks a gate, although conserved residues Glu47 and Arg135 in YaaE (Figure 5) may serve as a gate for PLP synthase.

Mechanistic Implications. A mechanistic proposal for the formation of PLP **4** from the lysine imine of RBP **7** and G3P **6** is outlined in Scheme 2. In this proposal, the RBP imine **7** undergoes a transimination with ammonia followed by dehydration and a tautomerization to give **10**. This then reacts with G3P **6** to give **11**. Tautomerization, followed by cyclization and loss of phosphate, gives **14**. A second dehydration tautomerization sequence gives **16**, which is converted to PLP **4** by a final dehydration/tautomerization. While the details of this complex condensation reaction

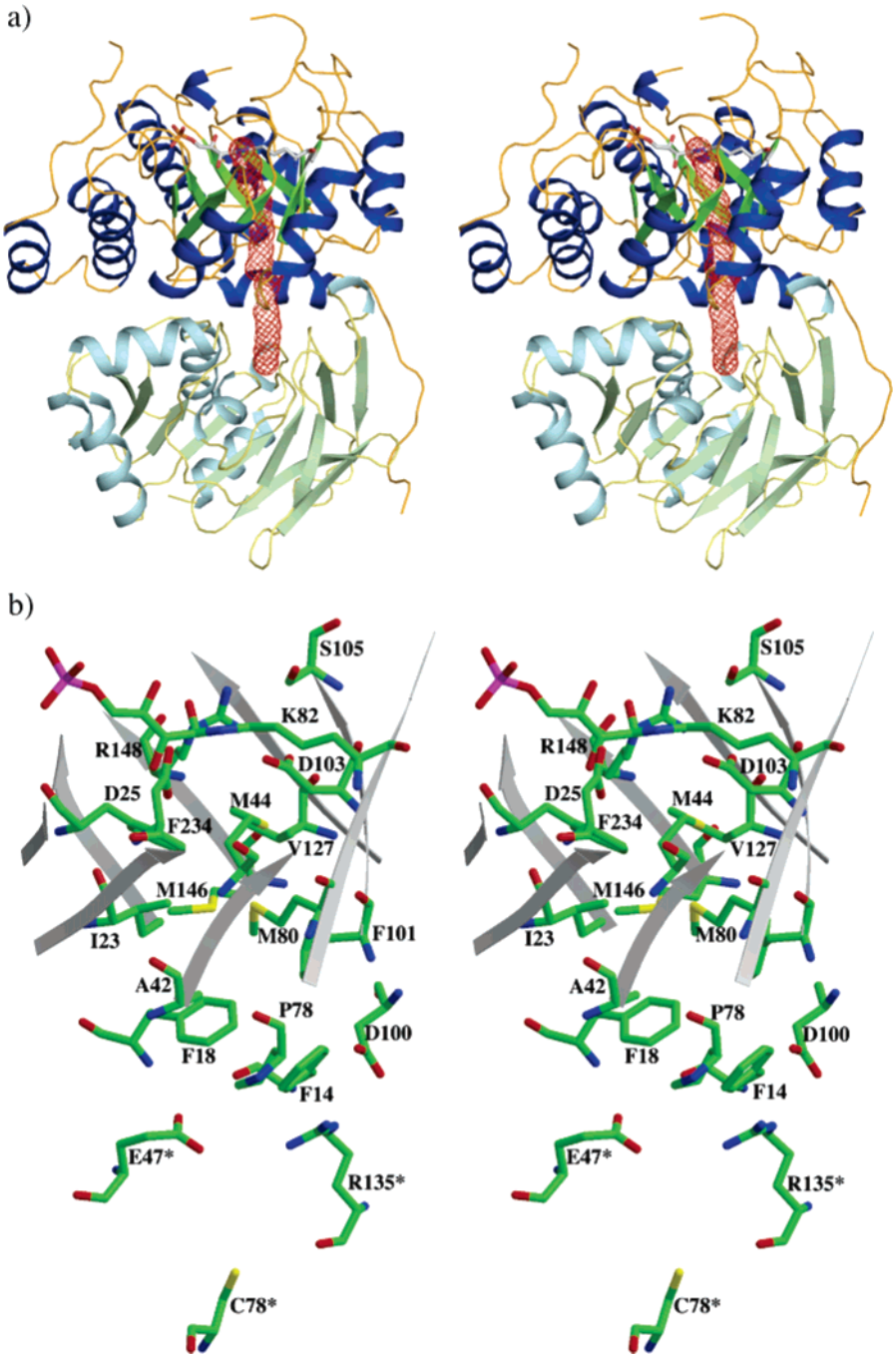

FIGURE 5: Putative ammonia channel. (a) Stereoview of a ribbons diagram of the YaaD−YaaE protomer. The red mesh indicates the path of the proposed ammonia channel. YaaD is color coded by secondary structure with α-helices shown in dark blue and *β*-strands in dark green. YaaE is color coded by secondary structure with α-helices shown in light blue and *β*-strands in light green. (b) Stereoview of amino acid residues that line the channel. Residues from YaaE are designated by asterisks. Ammonia is formed at the active site of YaaE (Cys78*) and travels across the YaaD−YaaE interface. The ammonia enters YaaD at the N-terminal end of the *β*-barrel (shown as gray ribbons). The channel is mostly hydrophobic until the RBP binding site is encountered.

Table 3: Properties of *B. subtilis* YaaD Mutants

	K81A	K149A
PLP formation	no	no
R5P isomerization	no	yes[a]
DHAP isomerization	yes	yes
adduct copurification	no	no[b]

[a] Three times faster than WT as determined by NMR analysis. [b] 60% adduct formation when given extra ribose 5-phosphate.

remain to be elucidated, the use of imine formation followed by a sequence of dehydration/tautomerization reactions for the formation of the pyridine heterocycle are likely to be constant features of any mechanistic proposal.

The RBP binding site of YaaD places the imine carbon of **7** at the end of the ammonia channel and suggests that Asp25 is the base involved in the conversion of **8** to **9** (Figure 4a). The structure also suggests that Asp103 and Arg148 are involved in the dehydration converting **16** to **17**. However, the functionality in the vicinity of Lys82 appears to be inadequate for the effective catalysis of the complex chemistry shown in Scheme 2. For example, the acid required to catalyze the dehydration converting **8** to **9** could not be identified, and the phosphate binding site involving hydrogen

Table 4: Comparison of YaaD with Known Protein Structures Using DALI (*44*)

protein	Z^a	RMSD[b] (Å)	LALI[c]	LSEQ2[d]	%IDE[e]
PdxS (1ZNN)	37.4	0.9	245	245	71
TIM (1HG3)	16.4	2.6	185	224	20
TPS (2TPS)	15.8	2.6	177	226	19
ThiG (1TYG)	15.2	2.6	183	242	20
PdxJ (1HO1)	15.1	2.9	182	235	11
TenI (1YAD)	14.5	2.5	168	190	15
HisHF (1JVN)	12.7	2.8	176	537	13

[a] Z-score (strength of structural similarity in standard deviations above expected). [b] Positional root-mean-square deviation of superimposed CA atoms in Å. [c] Total number of equivalenced residues. [d] Length of the entire chain of the equivalenced structure. [e] Percentage of sequence identity over equivalenced positions.

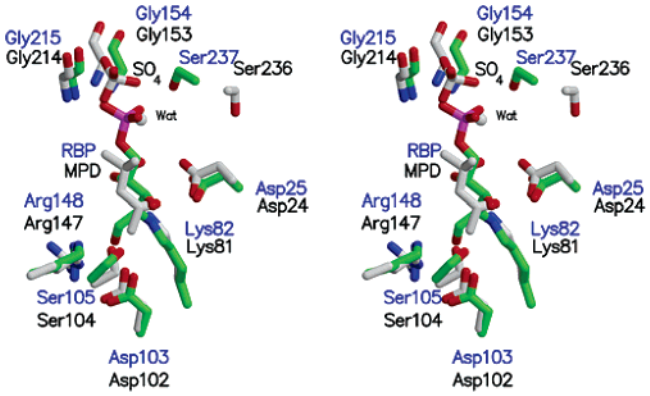

FIGURE 6: Stereoview of the superposition of the RBP site of YaaD and the MPD/sulfate site of PdxS. YaaD is shown with blue labels and green carbon atoms. PdxS is shown with black labels and gray carbon atoms. RBP, MPD, and sulfate are shown.

bonding interactions with the amide NH of Gly215, Gly154, Ser237, and Gly236 and the hydroxyl of Ser237 is not ideal for the stabilization of phosphate as a leaving group. In addition, there is no obvious binding site for G3P **6** or any clear constellation of acid/base residues required for its incorporation into PLP **4**. This suggests that the assembly of the PLP forming active site requires a major conformational change or that the RBP imine **7** is transferred to a different site for PLP formation. Studies on the *B. subtilis* PLP synthase described below lend support to this two-site model.

Previous ESI-FTMS studies on the *B. subtilis* PLP synthase localized a covalent R5P adduct to Lys149 (Lys150 in *T. maritima*) (*15*), while the crystal structure shows an imine between RBP and Lys82 (Lys81 in *B. subtilis*). To determine the function of these two lysine residues, the biochemical properties of the K81A and K149A mutants of the *B. subtilis* enzyme were analyzed. Both mutants were unable to catalyze the formation of PLP, demonstrating that each of these lysine residues plays an essential role in PLP formation. In addition, while the K81A mutant was unable to isomerize R5P to RBP, the K149A mutant catalyzed this isomerization at a rate that was three times faster than that of the native enzyme. These observations are consistent with a model in which the Lys81 containing site catalyzes the formation of the RBP imine from R5P. This imine is then transferred to the Lys149 containing site by a transimination reaction. The Lys149 site contains a cluster of conserved residues in a shallow cleft. The site also contains a phosphate ion in the *T. maritima* YaaD and a sulfate ion in PdxS (*22*). Although in the present structure Lys150 points away from the RBP binding site, modeling studies show that by side chain rotation and an approximately 1 Å shift of the main chain of Lys150 and conserved Gly151, the NZ atom can approach closely enough to RBP for the proposed transimination reaction to occur (Figure 9). Using Lys150 as a swinging arm allows the RBP to be repositioned such that the 5-phosphate occupies the conserved phosphate site.

The location of the ammonia channel suggests that access of ammonia to the Lys150 site is blocked by Asp25 and Arg148 (Figure 5). While this suggests that the ammonia molecule is utilized at the Lys82 active site, a result that would be inconsistent with the two-site model, the possibility that Asp25 and Arg148 form a gate that only opens after the transfer of RBP from Lys82 to Lys150 cannot be eliminated.

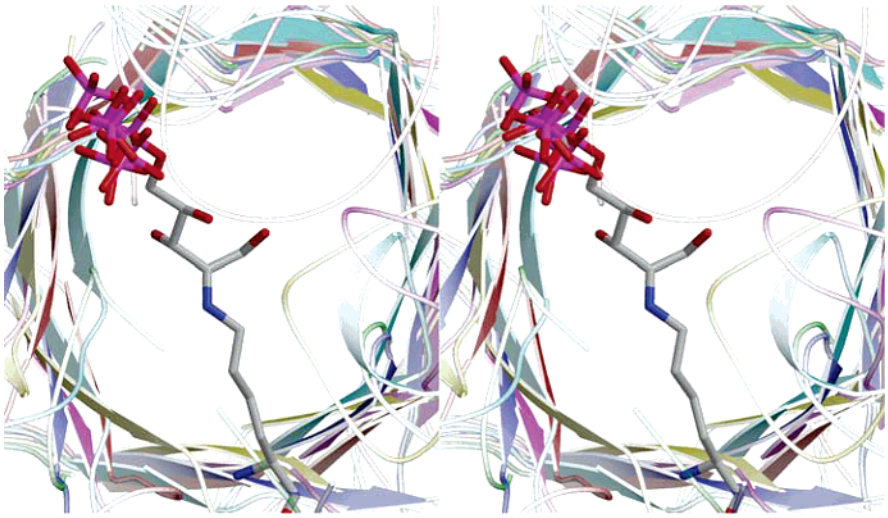

FIGURE 7: Stereoview of a conserved phosphate binding site in $(\beta/\alpha)_8$ barrels. The enzymes were identified by DALI (*44*) as being closely related to YaaD, while catalyzing different chemical reactions (except for PdxS). All atoms of RBP in YaaD are shown, but only the phosphate/sulfate groups for other substrates are pictured. The protein loops are white, and the β-strands are colored by protein. The color coding is YaaD (RBP)—green, PdxS (sulfate; 1ZNN)—blue, triose phosphate isomerase (2-carboxyethylphosphonic acid; 1HG3)—cyan, thiamin phosphate synthase (thiamin phosphate; 2TPS)—red; thiazole synthase (phosphate; 1TYG)—magenta, and pyridoxine 5′-phosphate synthase (PNP; 1HO4)—yellow.

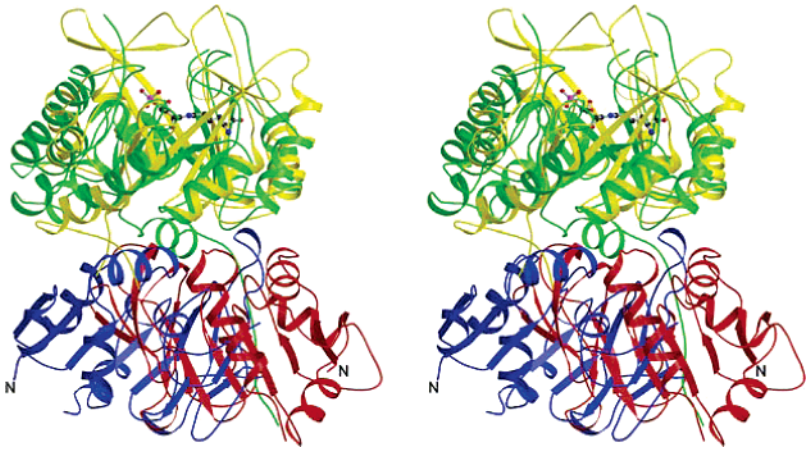

FIGURE 8: Superposition of HisHF and YaaD/YaaE. Only YaaD and HisF were used for the superposition. YaaD is shown in green; YaaE is shown in blue. HisF is shown in yellow, and HisH is shown in red. The covalently bound RBP ligand of YaaD is shown in ball-and-stick representation. The N-termini of YaaE and HisH are labeled, illustrating that the two glutaminase domains are rotated by about 180° with respect to each other.

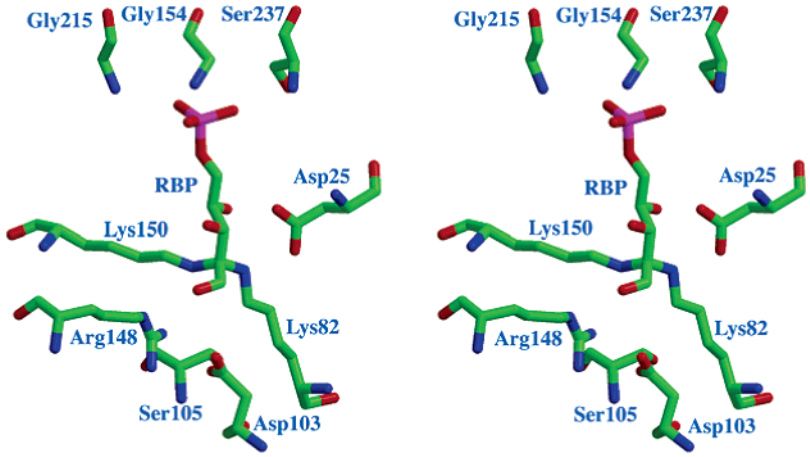

FIGURE 9: Model of a proposed Lys82/Lys150/RBP tetrahedral intermediate. The model shows how RBP could be transferred after isomerization between the Lys82 and Lys150 active sites.

Scheme 2

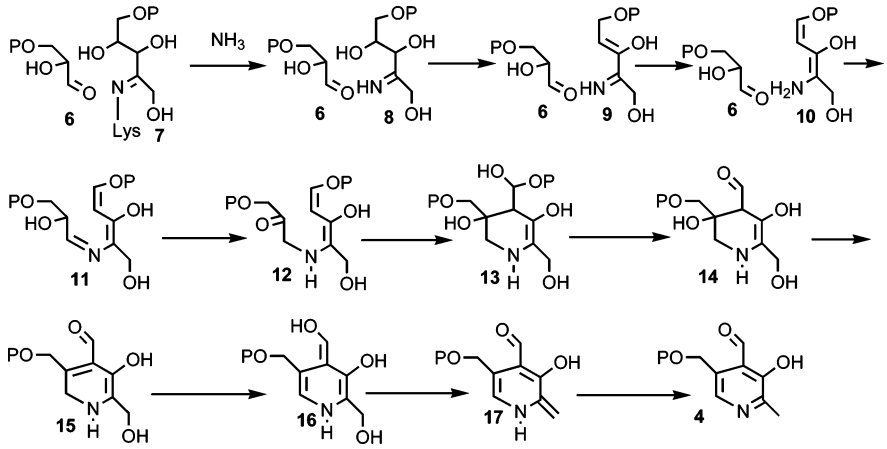

In conclusion, the structure of the PLP synthase complex suggests two YaaD active sites: one near Lys82 and one near Lys150. A cluster of conserved residues connects the two active sites, and either site can accommodate RBP and other intermediates. An ammonia channel runs through the YaaD β-barrel and connects the Lys82 active site to the glutaminase site of YaaE. While the PLP synthase complex provides new details for the alternate PLP biosynthetic pathway, the current structure does not identify the G3P binding site nor the binding sites of key reaction intermediates. The actual order of events in PLP biosynthesis and their structural localization will require further site-directed mutagenesis, biochemical analysis, and structural studies on enzyme intermediate and product complexes.

ACKNOWLEDGMENT

The authors wish to thank the NE-CAT beamline 24-ID-C at the Advanced Photon Source for provision of synchrotron

beam time. We thank Dr. Cynthia Kinsland for the YaaD and YaaE overexpression clones and Ms. Leslie Kinsland for assistance in the preparation of this manuscript.

REFERENCES

1. Eliot, A. C., and Kirsch, J. F. (2004) Pyridoxal phosphate enzymes: mechanistic, structural, and evolutionary considerations, *Annu. Rev. Biochem. 73*, 383−415.
2. John, R. A. (1998) Pyridoxal phosphate dependent enzymes, in *Comprehensive Biological Catalysis: A Mechanistic Reference* (Sinnott, M., Ed.) pp 173−200, Academic Press, San Diego, CA.
3. Mehta, P. K., and Christen, P. (2000) The molecular evolution of pyridoxal-5′-phosphate-dependent enzymes, *Adv. Enzymol. Relat. Areas Mol. Biol. 74*, 129−184.
4. Percudani, R., and Peracchi, A. (2003) A genomic overview of pyridoxal-phosphate-dependent enzymes, *EMBO Rep. 4*, 850−854.
5. Tanaka, T., Tateno, Y., and Gojobori, T. (2005) Evolution of vitamin B6 (pyridoxine) metabolism by gain and loss of genes, *Mol. Biol. Evol. 22*, 243−250.
6. Cane, D. E., Du, S. C., Robinson, J. K., Hsiung, Y., and Spenser, I. D. (1999) Biosynthesis of vitamin B-6: Enzymatic conversion of 1-deoxy-D-xylulose-5-phosphate to pyridoxol phosphate, *J. Am. Chem. Soc. 121*, 7722−7723.
7. Cane, D. E., Du, S. C., and Spenser, I. D. (2000) Biosynthesis of vitamin B-6: Origin of the oxygen atoms of pyridoxol phosphate, *J. Am. Chem. Soc. 122*, 4213−4214.
8. Zhao, G. S., and Winkler, M. E. (1995) Kinetic limitation and cellular amount of pyridoxine (pyridoxamine) 5′-phosphate oxidase of *Escherichia coli* K-12, *J. Bacteriol. 177*, 883−891.
9. Banks, J., and Cane, D. E. (2004) Biosynthesis of vitamin B-6: Direct identification of the product of PdxA-catalyzed oxidation of 4-hydroxy-L-threonine-4-phosphate using electrospray ionization mass spectrometry, *Bioorg. Med. Chem. Lett. 14*, 1633−1636.
10. Sivaraman, J., Li, Y. G., Banks, J., Cane, D. E., Matte, A., and Cygler, M. (2003) Crystal structure of *Escherichia coli* PdxA, an enzyme involved in the pyridoxal phosphate biosynthesis pathway, *J. Biol. Chem. 278*, 43682−43690.
11. Garrido-Franco, M., Laber, B., Huber, R., and Clausen, T. (2002) Enzyme-ligand complexes of pyridoxine 5′-phosphate synthase: implications for substrate binding and catalysis, *J. Mol. Biol. 321*, 601−612.
12. Yeh, J. I., Du, S. C., Pohl, E., and Cane, D. E. (2002) Multistate binding in pyridoxine 5′-phosphate synthase: 1.96 Å crystal structure in complex with 1-deoxy-D-xylulose phosphate, *Biochemistry 41*, 11649−11657.
13. Gupta, R. N., Hemscheidt, T., Sayer, B. G., and Spenser, I. D. (2001) Biosynthesis of vitamin B(6) in yeast: incorporation pattern of glucose, *J. Am. Chem. Soc. 123*, 11353−11359.
14. Zeidler, J., Gupta, R. N., Sayer, B. G., and Spenser, I. D. (2003) Biosynthesis of vitamin B(6) in yeast. Incorporation pattern of trioses, *J. Org. Chem. 68*, 3486−3493.
15. Burns, K. E., Xiang, Y., Kinsland, C. L., McLafferty, F. W., and Begley, T. P. (2005) Reconstitution and biochemical characterization of a new pyridoxal-5′-phosphate biosynthetic pathway, *J. Am. Chem. Soc. 127*, 3682−3683.
16. Belitsky, B. R. (2004) Physical and enzymological interaction of *Bacillus subtilis* proteins required for *de novo* pyridoxal 5′-phosphate biosynthesis, *J. Bacteriol. 186*, 1191−1196.
17. Bauer, J. A., Bennett, E. M., Begley, T. P., and Ealick, S. E. (2004) Three-dimensional structure of YaaE from *Bacillus subtilis*, a glutaminase implicated in pyridoxal-5′-phosphate biosynthesis, *J. Biol. Chem. 279*, 2704−2711.
18. Raschle, T., Amrhein, N., and Fitzpatrick, T. B. (2005) On the two components of pyridoxal 5′-phosphate synthase from *Bacillus subtilis*, *J. Biol. Chem. 280*, 32291−32300.
19. Ehrenshaft, M., Bilski, P., Li, M. Y., Chignell, C. F., and Daub, M. E. (1999) A highly conserved sequence is a novel gene involved in *de novo* vitamin B6 biosynthesis, *Proc. Natl. Acad. Sci. U.S.A. 96*, 9374−9378.
20. Ehrenshaft, M., and Daub, M. E. (2001) Isolation of PDX2, a second novel gene in the pyridoxine biosynthesis pathway of eukaryotes, archaebacteria, and a subset of eubacteria, *J. Bacteriol. 183*, 3383−3390.
21. Osmani, A. H., May, G. S., and Osmani, S. A. (1999) The extremely conserved pyroA gene of *Aspergillus nidulans* is required for pyridoxine synthesis and is required indirectly for resistance to photosensitizers, *J. Biol. Chem. 274*, 23565−23569.
22. Zhu, J., Burgner, J. W., Harms, E., Belitsky, B. R., and Smith, J. L. (2005) A new arrangement of $(\beta/\alpha)_8$ barrels in the synthase subunit of PLP synthase, *J. Biol. Chem. 280*, 27914−27923.
23. Mittenhuber, G. (2001) Comparative genomics and evolution of genes encoding bacterial (p)ppGpp synthetases/hydrolases (the Rel, RelA and SpoT proteins), *J. Mol. Microbiol. Biotechnol. 3*, 585−600.
24. Galperin, M. Y., and Koonin, E. V. (1997) Sequence analysis of an exceptionally conserved operon suggests enzymes for a new link between histidine and purine biosynthesis, *Mol. Microbiol. 24*, 443−445.
25. Zalkin, H., and Smith, J. L. (1998) Enzymes utilizing glutamine as an amide donor, *Adv. Enzymol. Relat. Areas Mol. Biol. 72*, 87−144.
26. Gengenbacher, M., Fitzpatrick, T. B., Raschle, T., Flicker, K., Sinning, I., Muller, S., Macheroux, P., Tews, I., and Kappes, B. (2006) Vitamin B6 biosynthesis by the malaria parasite *Plasmodium falciparum*: Biochemical and structural insights, *J. Biol. Chem. 281*, 3633−3641.
27. Otwinowski, Z., and Minor, W. (1997) Processing of x-ray diffraction data collected in oscillation mode, *Methods Enzymol. 276*, 307−326.
28. Brünger, A. T., Adams, P. D., Clore, G. M., DeLano, W. L., Gros, P., Grosse-Kunstleve, R. W., Jiang, J. S., Kuszewski, J., Nilges, M., Pannu, N. S., Read, R. J., Rice, L. M., Simonson, T., and Warren, G. L. (1998) Crystallography & NMR system: A new software suite for macromolecular structure determination, *Acta Crystallogr. D54*, 905−921.
29. Jones, T. A., Zou, J. Y., Cowan, S. W., and Kjeldgaard. (1991) Improved methods for building protein models in electron density maps and the location of errors in these models, *Acta Crystallogr. A47* (Part 2), 110−119.
30. Emsley, P., and Cowtan, K. (2004) Coot: Model-building tools for molecular graphics, *Acta Crystallogr. D60*, 2126−2132.
31. Kleywegt, G. J., and Jones, T. A. (1994) Halloween...mask and bones, in *From First Map to Final Model* (Bailey, S., Hubbard, R., and Waller, D., Eds.) pp 59−66, SERC Daresbury Laboratory, Warrington, U.K.
32. Laskowski, R. A., MacArthur, M. W., Moss, D. S., and Thornton, J. M. (1993) PROCHECK: A program to check the stereochemical quality of protein structures, *J. Appl. Crystallogr. 26*, 283−291.
33. Lovell, S. C., Davis, I. W., Arendall, W. B., 3rd, de Bakker, P. I., Word, J. M., Prisant, M. G., Richardson, J. S., and Richardson, D. C. (2003) Structure validation by Cα geometry: ϕ, ψ and Cβ deviation, *Proteins 50*, 437−450.
34. Kraulis, P. J. (1991) MOLSCRIPT: A program to produce both detailed and schematic plots of protein structures, *J. Appl. Crystallogr. 24*, 946−950.
35. Merritt, E. A., and Murphy, M. E. P. (1994) Raster 3D version 2.0 - A program for photorealistic molecular graphics, *Acta Crystallogr. D50*, 869−873.
36. DeLano, W. L. (2002) *The PyMOL Molecular Graphics System*, DeLano Scientific, San Carlos, CA.
37. Holm, L., and Sander, C. (1993) Protein structure comparison by alignment of distance matrices, *J. Mol. Biol. 233*, 123−138.
38. Walden, H., Bell, G. S., Russell, R. J., Siebers, B., Hensel, R., and Taylor, G. L. (2001) Tiny TIM: A small, tetrameric, hyperthermostable triosephosphate isomerase, *J. Mol. Biol. 306*, 745−757.
39. Chiu, H. J., Reddick, J. J., Begley, T. P., and Ealick, S. E. (1999) Crystal structure of thiamin phosphate synthase from *Bacillus subtilis* at 1.25 Å resolution, *Biochemistry 38*, 6460−6470.
40. Settembre, E. C., Dorrestein, P. C., Zhai, H., Chatterjee, A., McLafferty, F. W., Begley, T. P., and Ealick, S. E. (2004) Thiamin biosynthesis in *Bacillus subtilis*: Structure of the thiazole synthase/sulfur carrier protein complex, *Biochemistry 43*, 11647−11657.
41. Franco, M. G., Laber, B., Huber, R., and Clausen, T. (2001) Structural basis for the function of pyridoxine 5′-phosphate synthase, *Structure 9*, 245−253.

42. Chaudhuri, B. N., Lange, S. C., Myers, R. S., Chittur, S. V., Davisson, V. J., and Smith, J. L. (2001) Crystal structure of imidazole glycerol phosphate synthase: A tunnel through a $(\beta/\alpha)_8$ barrel joins two active sites, *Structure 9*, 987−997.
43. Douangamath, A., Walker, M., Beismann-Driemeyer, S., Vega-Fernandez, M. C., Sterner, R., and Wilmanns, M. (2002) Structural evidence for ammonia tunneling across the $(\beta/\alpha)_8$ barrel of the imidazole glycerol phosphate synthase bienzyme complex, *Structure 10*, 185−193.
44. Holm, L., and Sander, C. (1998) Touring protein fold space with Dali/FSSP, *Nucleic Acids Res. 26*, 316−319.

BI061464Y